Detection of multistability, bifurcations, and hysteresis in a large class of biological positive-feedback systems

David Angeli*, James E. Ferrell, Jr.[†], and Eduardo D. Sontag[‡§]

*Dipartimento di Sistemi e Informatica, University of Florence, 50139 Florence, Italy; [†]Departments of Molecular Pharmacology and Biochemistry, Stanford University School of Medicine, Stanford, CA 94305-5174; and [‡]Department of Mathematics, Rutgers, The State University of New Jersey, Hill Center, 110 Frelinghuysen Road, Piscataway, NJ 08854-8019

It is becoming increasingly clear that bistability (or, more generally, multistability) is an important recurring theme in cell signaling. Bistability may be of particular relevance to biological systems that switch between discrete states, generate oscillatory responses, or "remember" transitory stimuli. Standard mathematical methods allow the detection of bistability in some very simple feedback systems (systems with one or two proteins or genes that either activate each other or inhibit each other), but realistic depictions of signal transduction networks are invariably much more complex. Here, we show that for a class of feedback systems of arbitrary order the stability properties of the system can be deduced mathematically from how the system behaves when feedback is blocked. Provided that this open-loop, feedback-blocked system is monotone and possesses a sigmoidal characteristic, the system is guaranteed to be bistable for some range of feedback strengths. We present a simple graphical method for deducing the stability behavior and bifurcation diagrams for such systems and illustrate the method with two examples taken from recent experimental studies of bistable systems: a two-variable Cdc2/Wee1 system and a more complicated five-variable mitogen-activated protein kinase cascade.

Fig. 1. Feedback systems that may exhibit bistability. (*a*) A two-component positive-feedback loop, which can be analyzed by classical phase plane techniques. (*b*) A two-component, mutually inhibitory feedback loop, which can also be analyzed by classical phase plane techniques. (*c*) A longer mutually inhibitory feedback loop, which cannot be analyzed by classical phase plane techniques.

One of the most important and formidable challenges facing biologists and mathematicians in the postgenomic era is to understand how the behaviors of living cells arise out of the properties of complex networks of signaling proteins. One interesting systems-level property that even relatively simple signaling networks have the potential to produce is bistability. A bistable system is one that toggles between two discrete, alternative stable steady states, in contrast to a monostable system, which slides along a continuum of steady states (1–9). Early biological examples of bistable systems included the lambda phage lysis-lysogeny switch and the hysteretic lac repressor system (10–12). More recent examples have included several mitogen-activated protein kinase (MAPK) cascades in animal cells (13–15), and cell cycle regulatory circuits in *Xenopus* and *Saccharomyces cerevisiae* (16–18). Bistable systems are thought to be involved in the generation of switch-like biochemical responses (13, 14, 19), the establishment of cell cycle oscillations and mutually exclusive cell cycle phases (17, 18), the production of self-sustaining biochemical "memories" of transient stimuli (20, 21), and the rapid lateral propagation of receptor tyrosine kinase activation (22).

Bistability arises in signaling systems that contain a positive-feedback loop (Fig. 1*a*) or a mutually inhibitory, double-negative-feedback loop (which, in some regards, is equivalent to a positive-feedback loop) (Fig. 1*b*). Indeed, Thomas (23) conjectured that the existence of at least one positive-feedback loop is a necessary condition for the existence of multiple steady states; alternative proofs of this conjecture are given in refs. 24–27. However, the existence of positive loops is far from being sufficient; positive feedback does not guarantee bistability. A standard graphical test, termed phase plane analysis, can be used to visualize under what conditions a particular positive-feedback system will exhibit bistability, but this test is valid only if the system contains no more
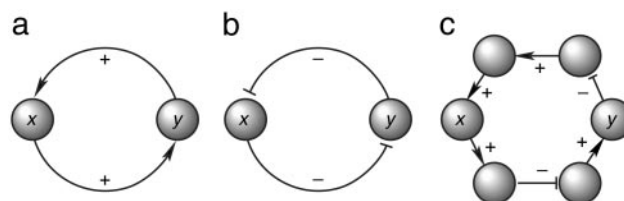
than two variables. Realistic biological networks generally contain more proteins and more variables (e.g., Fig. 1*c*), precluding the use of phase plane analysis.

Here, we present a method for analyzing positive-feedback systems of arbitrary order for the presence of bistability or multistability (i.e., more than two alternative stable steady states), bifurcation, and associated hysteretic behavior, subject to two conditions that are frequently satisfied even in complicated, realistic models of cell signaling systems: monotonicity and existence of steady-state characteristics (28–34). The main ideas of this article can be illustrated through two examples drawn from recent experimental studies: the Cdc2-cyclin B/Wee1 system, which can be considered to be a two-variable system, and the Mos/MAPK kinase p42 MAPK cascade, a five-variable system.

A Two-Variable Example: The Cdc2-Cyclin B/Wee1 System

As a first example, we will use our methods to determine the stability behavior and bifurcation diagram for a two-variable double-negative or mutually inhibitory feedback loop (Fig. 1*b*). Of course, this example can be treated without recourse to our theoretical developments, because it is generally straightforward to derive results for 2D systems through classical phase plane analysis (see *Supporting Text*, which is published as supporting information on the PNAS web site, for further discussion of the present method vs. phase plane analysis for two-variable systems). But precisely because it is possible to visualize phase plane behavior, the example affords us a way to compare our framework with classical approaches.

To put the example into concrete terms, we suppose that one of the proteins is the Cdc2-cyclin B complex, and the other is the Wee1 protein (Fig. 2*a*) (17, 18, 35–38), and we make a number of simplifications to allow the interplay between Cdc2-cyclin B and Wee1 to be treated as a two-variable problem. First, we assume that Cdc2-cyclin B and Wee1 each exist in only two forms (rather

---

Abbreviations: MAPK, mitogen-activated protein kinase; I/O, input/output.

[§]To whom correspondence should be addressed. E-mail: sontag@math.rutgers.edu.

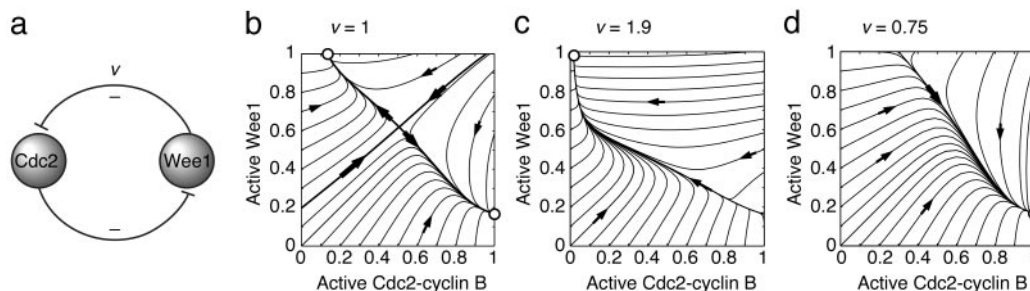© 2004 by The National Academy of Sciences of the USA

Fig. 2. Analysis of the Cdc2-cyclin B/Wee1 system by numerical simulation. (*a*) Schematic depiction of the system. (*b–d*) Phase plane plots of the Cdc2-cyclin B system. Constants are: $\alpha_1 = \alpha_2 = 1$, $\beta_1 = 200$, $\beta_2 = 10$, $\gamma_1 = \gamma_2 = 4$, $K_1 = 30$, $K_2 = 1$. Three different feedback gains are shown: $v = 1$ (*b*), $v = 1.9$ (*c*), and $v = 0.75$ (*d*).

multiple forms, as is actually the case): an active form (with x_1 denoting active Cdc2 and y_1 denoting active Wee1) and an inactive form (x_2 and y_2 denoting inactive Cdc2 and Wee1, respectively). Second, we assume that the phosphorylations of Cdc2 and Wee1 are reversed by some constitutively active phosphatases (which ignores the contribution of Cdc25 regulation to the bistability of the Cdc2 system). Finally, we assume that the inhibition of each kinase by the other is approximated by a Hill equation. The equations for this model system are:

$$\dot{x}_1 = \alpha_1 x_2 - \frac{\beta_1 x_1 (v y_1)^{\gamma_1}}{K_1 + (v y_1)^{\gamma_1}}, \quad \dot{x}_2 = -\alpha_1 x_2 + \frac{\beta_1 x_1 (v y_1)^{\gamma_1}}{K_1 + (v y_1)^{\gamma_1}}$$

$$\dot{y}_1 = \alpha_2 y_2 - \frac{\beta_2 y_1 x_1^{\gamma_2}}{K_2 + x_1^{\gamma_2}}, \quad \dot{y}_2 = -\alpha_2 y_2 + \frac{\beta_2 y_1 x_1^{\gamma_2}}{K_2 + x_1^{\gamma_2}}.$$

The αs and βs are rate constants; the Ks are Michaelis (saturation) constants; the γs are Hill coefficients; and v is a coefficient that reflects the strength of the influence of Wee1 on Cdc2-cyclin B, in control-theory terms, the "gain" of the system. (One could also define the gain of this feedback loop as $\partial x_1/\partial y_1$, or alternatively as $\partial \ln x_1/\partial \ln y_1$; all three measures provide a sense of the strength of the inhibition of Cdc2 by Wee1.) If we take $x_2 = 1 - x_1$ and $y_2 = 1 - y_1$ (that is, assume that the total concentrations of Wee1 and Cdc2-cyclin B are unchanging and measure concentrations in fractional terms), we can eliminate two variables from these equations and simplify them, yielding system **1**:

$$\dot{x}_1 = \alpha_1(1 - x_1) - \frac{\beta_1 x_1 (v y_1)^{\gamma_1}}{K_1 + (v y_1)^{\gamma_1}}, \quad \dot{y}_1 = \alpha_2(1 - y_1) - \frac{\beta_2 y_1 x_1^{\gamma_2}}{K_2 + x_1^{\gamma_2}}.$$

Phase Plane Diagrams for the Cdc2-Cyclin B/Wee1 System, Deduced from Numerical Simulations

We can then choose values for the constants α, β, κ, γ, and v, and numerically compute the time evolution of x_1 and y_1 for various choices of their initial values. As shown in Fig. 2*b*, when $v = 1$, the system exhibits bistability, with two attracting steady states, a high Cdc2-cyclin B-activity state (M phase-like) and a high Wee1 activity state (interphaselike), that essentially compete for trajectories. For values of $v > \approx 1.8$, only the low Cdc2-cyclin B/high Wee1 state persists (Fig. 2*c*), and the system changes from bistable to monostable. Likewise, for $v < \approx 0.83$, only the high Cdc2-cyclin B/low Wee1 state is present (Fig. 2*d*).

Global Stability Analysis of the Cdc2-Cyclin B/Wee1 System: The Open-Loop Approach

We will next explain how the bistability of the system at intermediate values of v, as well as the bifurcation diagram, can be deduced from the general theoretical framework presented in this article. This framework draws on the theory of monotone systems with

inputs and outputs. An outline of this theory is provided in *Supporting Text*; proofs and details can be found elsewhere (28, 29).

The key to our approach is to view system **1** as a feedback closure of the following open-loop system (**2**) in which the variable ω is seen as an input or "stimulus" variable, and $\eta = y_1$ is the output or "response" variable:

$$\dot{x}_1 = \alpha_1(1 - x_1) - \frac{\beta_1 x_1 \omega^{\gamma_1}}{K_1 + \omega^{\gamma_1}}, \quad \dot{y}_1 = \alpha_2(1 - y_1) - \frac{\beta_2 y_1 x_1^{\gamma_2}}{K_2 + x_1^{\gamma_2}}.$$

In other words, we analyze the system by "breaking" the feedback loop at the step of the inhibition of Cdc2 by Wee1, viewing the effect of Wee1 on Cdc2 as an input signal ω to be experimentally manipulated (Fig. 3 *a*), and only later, after analyzing the behavior of output η as a function of input ω, do we reclose the loop by letting $\omega = \eta$ (and hence recovering the original, intact, system).
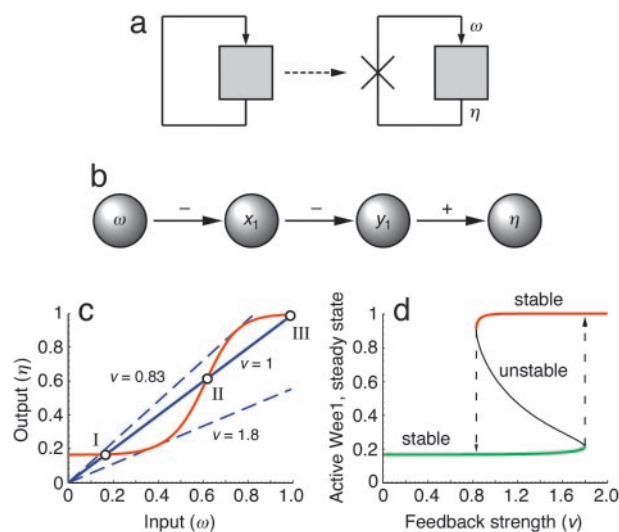

Fig. 3. Mathematical analysis of the Cdc2-cyclin B/Wee1 system, by breaking the feedback loop. (*a*) Schematic view of a feedback system before (*Left*) and after (*Right*) breaking the feedback loop. ω is the input of the open-loop system; η is the output. (*b*) Incidence graph for system **2**. (*c*) Steady-state I/O static characteristic curve (k_η is a function of ω) for system **2** (red), with constants chosen as in Fig. 2 *b–d*. The solid blue line represents ω as a function of η for unitary feedback. There are three intersection points (I, II, and III), which represent two stable steady states (I and III) and one unstable steady state (II). The dashed blue lines represent ω as a function of η for the values of the feedback gain v above which ($v \gtrsim 1.8$) and below which ($v \lesssim 0.83$) the system becomes monostable. (*d*) Bifurcation diagram for the system, showing bistability when the feedback strength v is between ≈ 0.83 and ≈ 1.8. The bifurcation diagram is obtained from the characteristic as the plot of the curve $[\omega/k(\omega), k(\omega)]$, with ω ranging over the allowed range of inputs.

BIOCHEMISTRY

Two critical properties are necessary for our methodology to apply, and they must be verified before the application of our theorem. These properties can be summarized as follows: (*A*) the open-loop system has a monostable steady-state response to constant inputs [we then say that the system has a well-defined steady-state input/output (I/O) characteristic]; and (*B*) there are no possible negative feedback loops, even when the system is closed under positive feedback (we then say that the system is strongly I/O monotone).

Property *A* means that, for each constant-in-time input signal $\omega(t) \equiv a$ for $t > 0$ (i.e., a step-function input stimulus), and for any initial conditions $x_1(0), y_1(0)$, the solution of the system of differential equations (**2**) converges to a unique steady state (which depends on the particular step magnitude a, but not on the initial states). When this property holds, we write $k_{x,y}(a)$ to indicate the steady-state vector $\lim_{t \to +\infty}[x_1(t), y_1(t)]$ corresponding to the signal $\omega(t) \equiv a$, and $k_\eta(a)$ to indicate the corresponding asymptotic value $\eta(+\infty)$ for the corresponding output signal.

One of the main steps in verifying the applicability of our analysis method to a particular system is that of checking that this property is satisfied. To a biochemist, property *A* might seem self-evident. However, it is not trivial to prove it rigorously, even for systems of differential equations that describe relatively simple signaling networks. In the example of the MAPK cascade treated later in this article, we appeal to a theorem proved in ref. 29 to establish this fact. But for system **2**, it is straightforward to verify the condition. For any constant input $\omega, k_\eta(\omega) = \eta(+\infty) = y_1(+\infty)$ is given by the following formula:

$$\frac{\alpha_2(K_2 + (\alpha_1(K_1 + \omega^{\gamma_1}))/(\alpha_1 K_1 + \alpha_1 \omega^{\gamma_1} + \beta_1 \omega^{\gamma_1}))^{\gamma_2}}{\alpha_2 K_2 + (\alpha_2 + \beta_2)(\alpha_1(K_1 + \omega^{\gamma_1})/(\alpha_1 K_1 + \alpha_1 \omega^{\gamma_1} + \beta_1 \omega^{\gamma_1}))^{\gamma_2}}.$$

This function has a single value for every value of ω; a plot of k_η is shown in Fig. 3*c* (red curve). Note the sigmoidal character of the curve, which is caused by our having assumed that $\gamma_1, \gamma_2 > 1$. This assumption will be critical for bistability.

The second of the properties to be verified before applying our theoretical results, property *B* (monotonicity), refers to the graphical structure of the interconnection among the dynamic variables. To make it precise, we introduce the incidence graph of a system, as follows (see Fig. 6, which is published as supporting information on the PNAS web site). For a system with n variables p_i, the incidence graph has $n + 2$ nodes (so, in the example in Eq. **2**, where $n = 2$, there are four nodes). The nodes are labeled ω, η, and p_i, $i = 1, \ldots, n$. A labeled edge (an arrow with a $+$ or $-$ sign attached to it) is drawn whenever a variable p_i (or input ω) affects directly the rate of change of a variable p_j (or the value of the output), and a sign is attached to each label: a $+$ sign whenever the effect is positive and $-$ if the effect is negative. If the effect is ambiguous, because the sign of its effect depends on the actual values of the input or state variables, then our method does not apply.

For our example **2**, the graph is shown in Fig. 3*b*. The negative arrow $\omega \to$ represents the fact that the function $\alpha_1(1 - x_1) - \beta_1 x_1 \omega^{\gamma_1}/(K_1 + \omega^{\gamma_1})$ in the first of the equations (**2**), which determines the rate of change of x_1, is a decreasing function of ω; i.e., ω inhibits x_1. The same holds for the influence of x_1 on y_1 (Eq. **2**). On the other hand, the choice of output $\eta = y_1$ is represented by a positive arrow. Autocatalytic or degradation effects (self-loops) are not reflected in the graph: for example, the decay term $-\alpha_1 x_1$ in the first equation makes the rate of change of x_1 be smaller if x_1 is greater, but it is not included in the graph.

Given any path in an incidence graph (such as the path ω, x_1, y_1 in the graph shown in Fig. 3*b*), we define its sign as the product of the signs along the path (in the example, the sign of ω, x_1, y_1 is positive, being the product of two negatives). We say that a path is positive or negative depending on its sign.

The property of monotonicity that we need amounts to checking these requirements: (*i*) every loop in the graph, directed or not, is positive; (*ii*) all of the paths from the input to the output node are positive; (*iii*) there is a directed path from the input node to each node p_i; and (*iv*) there is a directed path from each p_i to the output node. Note that *i* together with *ii* amounts to the requirement that every possible loop is positive, even after closing under any positive feedback. Properties *iii* and *iv* are technical conditions needed for mathematical reasons.

For our example, *i* is automatically verified (there are no loops), and *ii–iv* are obvious from the graph shown in Fig. 3*b*. Thus both the prerequisite conditions *A* and *B* are satisfied for the example system (**2**), and our method can be applied.

The next step consists of graphing together the characteristic k_η, which represents the steady-state output η as a function of the constant input ω (Fig. 3*c*, red line), with the diagonal $\eta = \omega$, which represents ω as a function of (Fig. 3*c*, blue line). Algebraically, this amounts to looking for fixed points of the mapping k_η. We find that there are three intersections between these graphs, which we will refer to as points I, II, and III, respectively. At each of the three points of intersection, we consider the slope of the characteristic k and ask whether the slope is greater than unity or not. We see from the picture that this slope is <1 at I and III and >1 at II.

Our theorem then concludes as follows. First, in the state-space of the closed-loop system (**1**), which is obtained by writing $\omega = \eta = y_1$ in the system **2**, there are three steady states, let us call them x_{I}, x_{II}, and x_{III}, respectively, corresponding to the I/O pairs associated to the points I, II, and III. Second, the states x_{I} and x_{III}, which correspond to the points at which the characteristic has slope <1, are attracting (that is to say, stable) steady states, whereas x_{II} is unstable. Finally, we can conclude that every trajectory, except possibly for an exceptional set of zero measure, converges to either x_{I} or x_{III}. Clearly, these conclusions are consistent with the phase plane shown in Fig. 2*b*, which shows two stable states, whose domains of attraction span the whole positive orthant (with the exception of the separatrix corresponding to the stable manifold of the unstable state, a saddle). This is not only true for a simple two-component system like the one illustrated in Eq. **1**, but also for any *n*-component system satisfying our monotonicity and open-loop steady-state response assumptions.

Note that if the characteristic k_η had not been sigmoidal (if we had assumed both of the Hill coefficients to be 1 or less) there could not be three intersections, and the system could not be bistable at any feedback strength. This finding suggests an experimental approach to the detection of bistability in positive-feedback systems. If the feedback can be blocked in such a system, and if the feedback-blocked system is known (or correctly intuited) to be monotone, then if the experimentally determined steady-state stimulus/response curve of the feedback-blocked system is sigmoidal, the full feedback system is guaranteed to be bistable for some range of feedback strengths. Conversely, if the open-loop system exhibits a linear response, a Michaelian response, or any response that lacks an inflection point, the feedback system is guaranteed to be monostable despite its feedback. Thus, some degree of "cooperativity" or "ultrasensitivity" is essential for bistability in monotone systems of any order.

The bifurcation diagram for the Cdc2-cyclin B/Wee1 system, a plot of the possible steady states as a function of the feedback strength v, can be determined from the properties of the open-loop system as well. To do this, we study the effect of a feedback law $\omega = v \times \eta$ which amounts to intersecting the characteristic k_η with lines $\eta = (1/v)\omega$, as shown in Fig. 3*d* for $v = 0.83$ and $v = 1.8$. Observe that, for $v < \approx 0.83$ there is only one intersection (a high Cdc2-cyclin B, low Wee1 state), and for $v > \approx 1.8$ there will again be just one intersection (a low Cdc2-cyclin B, high Wee1 state) (Fig. 3*d*, dashed lines). In both cases, our theorem predicts a unique globally asumptotically stable steady state in the full system, consistently with the phase planes corresponding to $v = 1.9$ and $v = 0.75$ shown, respectively, in Fig. 2 *c* and *d*. In the intermediate range, there will be three intersections, one associated with an unstable
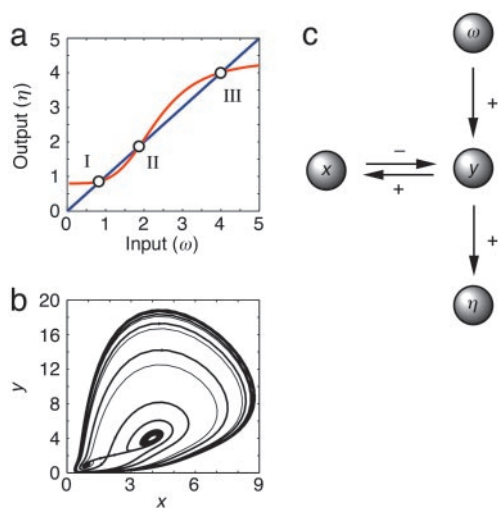
Fig. 4. Analysis of a system with similar-looking characteristic curves (compare Fig. 3c) but qualitatively different stability behavior. (a) Steady-state I/O static characteristic curve for system **4**. Constants are: $c = 0.8$, $b = 500/140$, $K = 405/14$. (b) Phase plane for system **4**. (c) Incidence graph for system **4**.

state and the others with stable states. Thus, one recovers the complete bifurcation diagram (Fig. 3d) from the graph of the I/O steady-state characteristic, not using numerical methods, and even if no detailed mathematical model is available.

Finally, the hysteretic behavior of the system can be deduced from Fig. 3d: increasing v from low to high results in picking the lower branch in the bistable regime, whereas decreasing from high to low takes us on the upper branch.

Monotonicity Is Needed

We should emphasize that the monotonicity assumption B is absolutely essential for the validity of our results. The conclusion that stable states will be in a one-to-one correspondence with points at which the steady-state I/O characteristic intersects the diagonal $\eta = \omega$ with slope <1 is, in general, false. To illustrate the need for monotonicity, let us consider the following example. We take the system described by these equations (**4**):

$$\dot{x} = x(-x + y), \quad \dot{y} = 3y\left(-x + c + \frac{by^4}{k + y^4}\right)$$

with output $\eta = y$. This system models a situation in which two proteins x and y, whose concentrations are denoted by $x(t)$ and $y(t)$, respectively, interact as follows. Protein x can be degraded when it is dimeric (hence the $-x^2$ term in the first differential equation), and its formation is promoted by protein y (term xy). Protein y is degraded by x (term $-xy$ in the second equation) and its synthesis is driven by cooperative autocatalysis (positive feedback of y upon itself, last term). The state space on which this system evolves is the positive orthant ($x > 0$ and $y > 0$). This is an activator/inhibitor system and corresponds to a predator–prey system from population biology and ecology. To apply our methodology, we view the system as the unitary feedback system that results from setting $\omega = \eta = y$ in the following open-loop system:

$$\dot{x} = x(-x + y), \quad \dot{\eta} = \dot{y} = 3y\left(-x + c + \frac{b\omega^4}{K + \omega^4}\right).$$

This system admits a well-defined steady-state I/O static characteristic k_η given by: $k_\eta(\omega) = c + b\omega^4/(K+\omega^4)$ and plotted, for a particular choice of constants, in Fig. 4a. Note that this characteristic curve is qualitatively very similar to that shown in Fig. 3c. Following our method, we intersect the graph of k_η with the

diagonal, find three intersection points, and classify the three associated steady states of the system according to the slopes at the intersection. Because there are two intersections with slope <1 and one with slope >1, we conclude (erroneously, as it turns out) that there are two stable steady states, to which all trajectories (except for those in the stable manifold of the one unstable state) converge. This conclusion is totally false, as evidenced by the phase plane of the system, shown in Fig. 4b. Trajectories do not converge to one of two stable states, as expected for a bistable system. In fact, the system has no stable steady states, and there is instead a limit cycle oscillation. The failure of the system to exhibit the "expected" bistability is due to the fact that the system is not monotone. As shown by its incidence graph (Fig. 4c), the loop x, y, x is negative.

The Modularity of Monotone Systems

One approach to complex cell signaling networks is to divide the network into subsystems or modules of a more tractable size and hope that the behavior of the entire system can be deduced from the behaviors of these modules (39, 40). However, in real biological networks there are interconnections between modules, and under such circumstances there is no general guarantee that the behavior of an isolated module will bear any resemblance to the behavior of the module in its natural context. Thus, although modularity remains a potentially important and highly desirable property of cell signaling networks, it is not certain whether modularity is rare or commonplace.

However, it is straightforward to show that any cascade composed of subsystems, each of which is monotone and admits a well-defined characteristic, will itself be monotone and admit a characteristic (28, 29). Thus, there is an intrinsic modularity to monotone systems, which is important both conceptually and in terms of devising approaches to the dissection of complex signaling systems. We make use of this modularity in the example that follows.

A Modular, Five-Variable Example: The Mos/MEK/p42 MAPK Cascade

Here, we use our approach to analyze a higher dimensional system drawn from the experimental literature. The system is a three-tier MAPK cascade, based on the Mos/MEK1/p42 MAPK cascade present in *Xenopus* oocytes (Fig. 5a). This particular MAPK cascade was chosen for several reasons: the cascade is known to be embedded in a positive-feedback loop (41–43) and to exhibit bistability (13, 21); all of the relevant protein abundances and some of the important kinetic parameters have been measured (44–46); and experimental studies have been performed on the cascade both as a closed-loop system (the normal situation) and an open-loop system (where the feedback from p42 MAPK to Mos has been blocked) (13, 47).

The key features of the cascade are shown schematically in Fig. 5a. Active Mos (x) accumulates based on a balance between synthesis and degradation and can activate MEK through phosphorylation of two residues (converting unphosphorylated y_1 to monophosphorylated y_2 and then bisphosphorylated y_3). Active MEK then phosphorylates p42 MAPK (z_1) at two residues, resulting in p42 MAPK activation. Active p42 MAPK (z_3) can then promote Mos synthesis, completing the closed positive-feedback loop. In addition, each of the phosphorylation reactions is opposed by an unregulated dephosphorylation reaction. Details on the rationale behind this model and the assumed protein abundances and kinetic constants are provided in *Supporting Text* and Table 1, which is published as supporting information on the PNAS web site.

We mathematically model the dynamics of the cascade by means of a system of seven differential equations (cf. refs. 47 and 48), using $x(t)$ to denote the concentration of Mos at time t, $y_1(t)$ to denote the concentration of unphosphorylated MEK at time t, and so on, as illustrated in Fig. 5a (see *Supporting Text* for the equations). We will view this system as the closure under feedback $\omega = vz_3$ of the
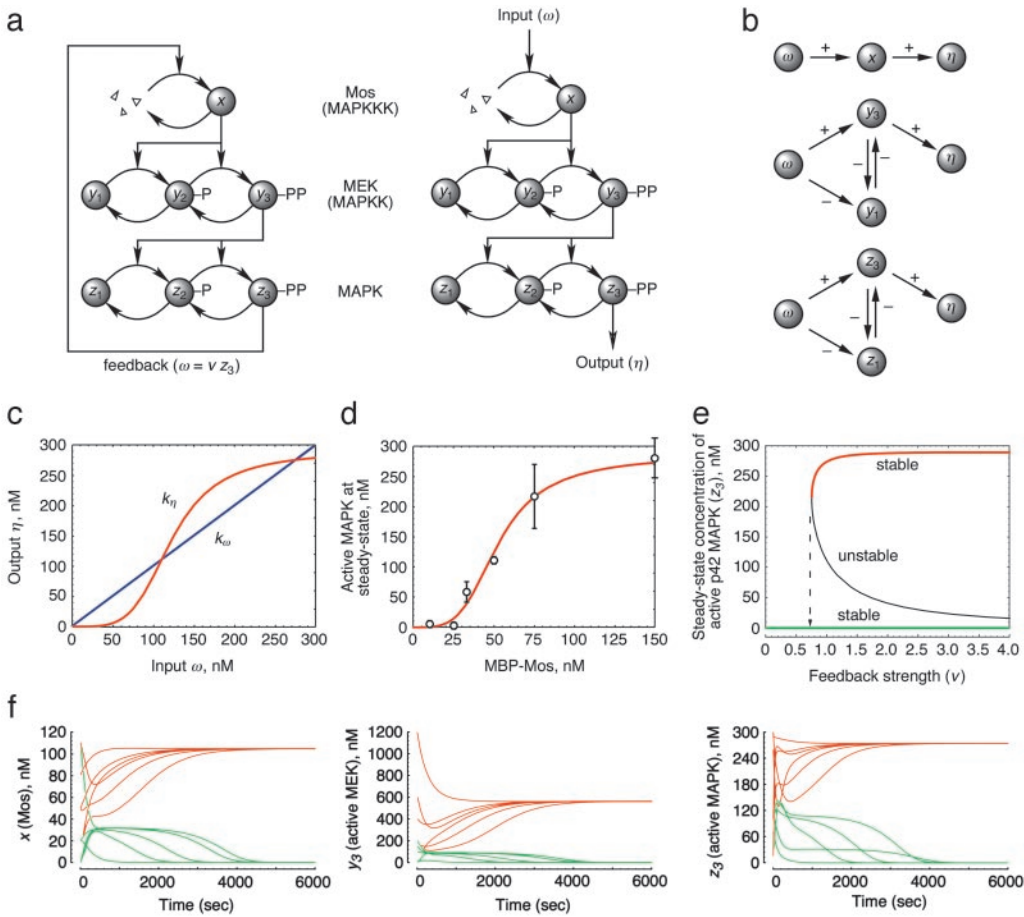
Fig. 5. Bistability in a MAPK cascade. (*a*) Schematic depiction of the Mos-MEK-p42 MAPK cascade, a linear cascade of protein kinases embedded in a positive-feedback loop (*Left*), together with the corresponding open-loop system (*Right*). (*b*) Incidence graph for a 2D subsystem (a single level) of a kinase cascade. (*c*) Steady-state I/O characteristic (k_η as a function of ω) for the MAPK cascade (red curve), plotted together with the diagonal, representing ω as a function of η with unity feedback (blue line). (*d*) Experimental demonstration of a sigmoidal response of MAPK to Mos. Experimental data are taken from ref. 47 and are means ± SD. (*e*) Bifurcation diagram for the MAPK cascade, showing the stable on-state (red curve), the stable off-state (green curve), and the unstable threshold (black curve) as a function of feedback strength (*v*). (*f*) Simulations show that trajectories funnel toward one of two stable steady states, denoted by red and green ticks, as required by our theorem. Shown are calculated concentrations of Mos (*x*), active MEK (y_3), and active MAPK (z_3) for 11 choices of initial conditions, as a function of time.

open-loop system that results when ω is substituted for vz_3 in the first equation. Furthermore, we have the following two conservation laws: MEK + MEK-P + MEK-PP = MEK$_{tot}$ = 1,200 nM = y_1 + y_2 + y_3, and MAPK + MAPK-P + MAPKPP = MAPK$_{tot}$ = 300 nM = z_1 + z_2 + z_3, which we can use to reduce the original seven equations to the following system of five differential equations (**6**):

$$\dot{x} = -\frac{V_2 x}{K_2 + x} + V_0 \omega x + V_1$$

$$\dot{y}_1 = \frac{V_6(1200 - y_1 - y_3)}{K_6 + (1200 - y_1 - y_3)} - \frac{V_3 x y_1}{K_3 + y_1}$$

$$\dot{y}_3 = \frac{V_4 x(1200 - y_1 - y_3)}{K_4 + (1200 - y_1 - y_3)} - \frac{V_5 y_3}{K_5 + y_3}$$

$$\dot{z}_1 = \frac{V_{10}(300 - z_1 - z_3)}{K_{10} + (300 - z_1 - z_3)} - \frac{V_7 y_3 z_1}{K_7 + z_1}$$

$$\dot{z}_3 = \frac{V_8 y_3(300 - z_1 - z_3)}{K_8 + (300 - z_1 - z_3)} - \frac{V_9 z_3}{K_9 + z_3}.$$

We will now use our methodology to analyze this system. The first step is to view system **6** as a cascade of three modular subsystems: the 1D x (Mos) system, whose input is ω and output is x; the 2D y_1, y_3 (MEK) system, whose input is x and output is y_3; and the 2D z_1, z_3 (MAPK) system, whose input is y_3 and output is z_3.

It is straightforward to see that the first (Mos) level of the cascade admits a well-defined I/O characteristic, and in refs. 28 and 29 it was proved that the MEK and MAPK subsystems do as well; thus, the entire cascade admits a well-defined I/O characteristic, and prop-

erty *A* is satisfied. Next, monotonicity needs to be verified. This is trivial for the first subsystem, whose incidence graph is shown in Fig. 5*b*. For each of the two 2D subsystems (the dual phosphorylation of MEK and the dual phosphorylation of p42 MAPK) the incidence graph is more complicated, but again the monotonicity of these subsystems can be inferred by inspection (Fig. 5*b* and *Supporting Text*). Because each subsystem in the cascade is monotone, the entire cascade is guaranteed to be monotone as well, and property *B* is satisfied. Thus, all our theoretical considerations can be applied to the system described by Eq. **6**.

Next, we numerically calculate the steady-state I/O characteristic, k_η, for the model system. As shown in Fig. 5*c*, the curve is steeply sigmoidal, similar in shape to a Hill equation curve with a Hill coefficient of 5. In our model the sigmoidal character of the characteristic arises mostly from the assumed nonprocessive dual phosphorylation mechanisms for MAPK and MEK activation (49, 50). As described in *Supporting Text*, the parameters for the model were chosen to reproduce the experimentally observed sigmoidal relationship for MAPK activity as a function of Mos concentration in an open-loop (feedback-blocked) system (47), lending confidence that the I/O characteristic curve for the Mos/MEK/p42 MAPK system is, in fact, sigmoidal, as it is in our model.

Accordingly, we can deduce the global stability behavior of the entire five-dimensional system from a plot of the characteristic k_η, and the line $\omega = vz_3$. Under unitary feedback ($v = 1$), the system has three steady states (Fig. 5*c*), and our theoretical framework allows us to conclude that the middle one is unstable and the high and low states are stable. Moreover, every trajectory (except for a zero-measure separatrix corresponding to the stable manifold of the unstable steady state) must necessarily converge to one of the two stable states.

Angeli *et al*.

The mathematically proven bistability of the MAPK cascade model can be illustrated through numerical simulations. We chose 11 sets of initial conditions for system **6** and solved the differential equations numerically (under unity feedback). Fig. 5*f* shows the time evolution of three of the variables (x, the concentration of Mos; y_3, the concentration of active MEK; and z_3, the concentration of active MAPK). As required by our theorem, all of the variables funnel into one of two discrete, five-dimensional stable steady states: an "on-state" (with most of the Mos and MAPK active and about half of the MEK active) and an "off-state" (with very low concentrations of active Mos, MEK, and MAPK).

If the feedback gain is not necessarily equal to one, we obtain the stability behavior of the system by intersecting the I/O characteristic with the line of slope $1/v$. The result is that the system is monostable when v is $< \approx 0.7$ (the on-state vanishes) or when v is very large (the off-state vanishes) and is bistable for any value of v in between. Therefore, the bistability of this model system is a fairly robust function of the feedback gain.

Experimental Studies

One key question is whether the Mos/MEK/p42 MAPK cascade actually does exhibit a sigmoidal stimulus response curve, resembling the characteristic k_η of the model system, when feedback is blocked. If it does, and if the system really is monotone (as is true for the model), then it is mathematically guaranteed that the closed-loop system will be bistable for some range of feedback strengths, irrespective of the exact details and parameters of the system. Experimental data are not yet available for the complete open-loop system (the experiment is difficult to perform), but data are available for the response of p42 MAPK to different concentrations of Mos in the absence of feedback (47). The steady-state activity of p42 MAPK as a function of the concentration of added recombinant Mos was found to be steeply sigmoidal (Fig. 5*d*), and the model agrees well with the experimental data (Fig. 5*d*, line). The steeply sigmoidal shape for the open-loop Mos/p42 MAPK curve supports the notion that the closed-loop feedback system should exhibit bistability, and indeed there is ample experimental evidence that when feedback is permitted, this system does exhibit a bistable response (13).

More Complicated Types of Feedback

Thus far we have analyzed systems where the output feeds back directly to the input. More complicated feedback loops may also be studied by using the same basic approach, by a reduction to unity feedback. This is discussed further in *Supporting Text* and Fig. 7, which is published as supporting information on the PNAS web site.

Summary

We have shown that for a large class of biological positive-feedback systems of arbitrary order it is possible to determine whether the system exhibits bistability, bifurcations, and hysteretic stimulus/response relationships mathematically, without recourse to extensive numerical simulations. This analysis can be implemented as a simple graphical method: a characteristic curve (for the open-loop system) and a straight line (which essentially equates the input of the open-loop system with the output) are plotted on one set of axes; the intersection points determine the steady states of the system; and the relative slopes of the two lines at the intersection points determine the stability of the steady states. Moreover, this same type of analysis can be implemented as an experimental program: if it is possible to measure the steady-state I/O relationship for a feedback loop under conditions where the feedback is blocked (e.g., by inhibitors, small interfering RNAs, or other experimental manipulations), and it can be demonstrated or safely assumed that the system is monotone, then the system's stability behavior can be rigorously inferred from the shape of the I/O curve, irrespective of the details of the biochemical mechanism that led to produced the curve. Our hope is that this method will help us to analyze and understand the mechanistic basis of important systems-level biological behaviors.

1. Glansdorff, P. & Prigogine, I. (1971) *Thermodynamics of Structure, Stability, and Fluctuations* (Wiley, New York).
2. Meyer, T. & Stryer, L. (1988) *Proc. Natl. Acad. Sci. USA* **85,** 5051–5055.
3. Segel, L. A. (1998) *Biophys. Chem.* **72,** 223–230.
4. Smolen, P., Baxter, D. A. & Byrne, J. H. (1998) *Am. J. Physiol.* **274,** C531–C542.
5. Laurent, M. & Kellershohn, N. (1999) *Trends Biochem. Sci.* **24,** 418–422.
6. Ferrell, J. E., Jr., & Xiong, W. (2001) *Chaos* **11,** 227–236.
7. Thomas, R. & Kaufman, M. (2001) *Chaos* **11,** 170–179.
8. Gardner, T. S., Cantor, C. R. & Collins, J. J. (2000) *Nature* **403,** 339–342.
9. Becskei, A., Seraphin, B. & Serrano, L. (2001) *EMBO J.* **20,** 2528–2535.
10. Novick, A. & Wiener, M. (1957) *Proc. Natl. Acad. Sci. USA* **43,** 553–566.
11. Cohn, M. & Horibata, K. (1959) *J. Bateriol.* **78,** 601–612.
12. Ptashne, M. (1992) *A Genetic Switch: Phage and Higher Organisms* (Blackwell, Oxford).
13. Ferrell, J. E., Jr., & Machleder, E. M. (1998) *Science* **280,** 895–898.
14. Bagowski, C. P. & Ferrell, J. E. (2001) *Curr. Biol.* **11,** 1176–1182.
15. Bhalla, U. S., Ram, P. T. & Iyengar, R. (2002) *Science* **297,** 1018–1023.
16. Cross, F. R., Archambault, V., Miller, M. & Klovstad, M. (2002) *Mol. Biol. Cell* **13,** 52–70.
17. Sha, W., Moore, J., Chen, K., Lassaletta, A. D., Yi, C. S., Tyson, J. J. & Sible, J. C. (2003) *Proc. Natl. Acad. Sci. USA* **100,** 975–980.
18. Pomerening, J. R., Sontag, E. D. & Ferrell, J. E., Jr. (2003) *Nat. Cell Biol.* **5,** 346–351.
19. Bagowski, C. P., Besser, J., Frey, C. R. & Ferrell, J. E., Jr. (2003) *Curr. Biol.* **13,** 315–320.
20. Lisman, J. E. (1985) *Proc. Natl. Acad. Sci. USA* **82,** 3055–3057.
21. Xiong, W. & Ferrell, J. E., Jr. (2003) *Nature* **426,** 460–465.
22. Reynolds, A. R., Tischer, C., Verveer, P. J., Rocks, O. & Bastiaens, P. I. (2003) *Nat. Cell Biol.* **5,** 447–453.
23. Thomas, R. (1981) in *Quantum Noise*, Springer Series in Synergetics 9, ed. Gardiner, C. W. (Springer, Berlin), pp. 180–193.
24. Snoussi, E. H. (1998) *J. Biol. Sys.* **6,** 3–9.
25. Plahte, E., Mestl, T. & Omholt, W. S. (1995) *J. Biol. Sys.* **3,** 409–413.
26. Gouzé, J. L. (1998) *J. Biol. Sys.* **6,** 11–15.
27. Cinquin, O. & Demongeot, J. (2002) *J. Theor. Biol.* **216,** 229–241.
28. Angeli, D. & Sontag, E. D. (2003) *Syst. Control Lett.*, in press.
29. Angeli, D. & Sontag, E. D. (2003) *IEEE Trans. Autom. Control* **48,** 1684–1698.
30. Hirsch, M. (1983) in *Differential Equations and Convergence Almost Everywhere in Strongly Monotone Flows*, ed. Smoller, J. (Am. Math. Soc., Providence, RI), pp. 267–285.
31. Hirsch, M. (1985) *SIAM J. Math. Anal.* **16,** 423–439.
32. Smale, S. (1976) *J. Math. Biol.* **3,** 5–7.
33. Smith, H. L. (1995) *Monotone Dynamical Systems: An Introduction to the Theory of Competitive and Cooperative Systems* (A. Math. Soc., Providence, RI).
34. Sontag, E. D. (1998) *Mathematical Control Theory: Deterministic Finite Dimensional Systems* (Springer, New York).
35. Thron, C. D. (1996) *Biophys. Chem.* **57,** 239–251.
36. Masui, Y. & Markert, C. L. (1971) *J. Exp. Zool.* **177,** 129–145.
37. Hunt, T. (1991) *Semin. Cell. Biol.* **2,** 213–222.
38. Novak, B. & Tyson, J. J. (1993) *J. Cell Sci.* **106,** 1153–1168.
39. Hartwell, L. H., Hopfield, J. J., Leibler, S. & Murray, A. W. (1999) *Nature* **402,** C47–C52.
40. Bhalla, U. S. & Iyengar, R. (2001) *Novartis Found. Symp.* **239,** 4–13.
41. Matten, W. T., Copeland, T. D., Ahn, N. G. & Vande Woude, G. F. (1996) *Dev. Biol.* **179,** 485–492.
42. Gotoh, Y., Masuyama, N., Dell, K., Shirakabe, K. & Nishida, E. (1995) *J. Biol. Chem.* **270,** 25898–25904.
43. Roy, L. M., Haccard, O., Izumi, T., Lattes, B. G., Lewellyn, A. L. & Maller, J. L. (1996) *Oncogene* **12,** 2203–2211.
44. Ferrell, J. E., Jr. (1996) *Trends Biochem. Sci.* **21,** 460–466.
45. Sohaskey, M. L. & Ferrell, J. E., Jr. (1999) *Mol. Biol. Cell* **10,** 3729–3743.
46. Mansour, S. J., Candia, J. M., Matsuura, J. E., Manning, M. C. & Ahn, N. G. (1996) *Biochemistry* **35,** 15529–15536.
47. Huang, C.-Y. F. & Ferrell, J. E., Jr. (1996) *Proc. Natl. Acad. Sci. USA* **93,** 10078–10083.
48. Kholodenko, B. N. (2000) *Eur. J. Biochem.* **267,** 1583–1588.
49. Ferrell, J. E., Jr., & Bhatt, R. R. (1997) *J. Biol. Chem.* **272,** 19008–19016.
50. Burack, W. R. & Sturgill, T. W. (1997) *Biochemistry* **36,** 5929–5933.

BIOCHEMISTRY

Supporting Text

Theoretical Foundations. Here, we describe the general theoretical framework that underlies our methodology; proofs and details can be found in refs. 1 and 2.

Our results apply to systems of ordinary differential equations of the following general form:

$$
\begin{aligned}
\dot{x}_1 &= f_1(x_1, \ldots, x_n, \omega) \\
\dot{x}_2 &= f_2(x_1, \ldots, x_n, \omega) \\
&\vdots \\
\dot{x}_n &= f_n(x_1, \ldots, x_n, \omega),
\end{aligned}
$$

which describe the evolution of a set of variables $x_1(t), \ldots, x_n(t)$; ω represents an external "input" signal that may be applied to the system. (In this article, ω is always a scalar quantity, but extensions of our results to vector quantities are possible; see refs. 1 and 2.) In addition, we suppose that an "output" variable η, which is a function $\eta = h(x)$ of the vector of state variables $x = (x_1, \ldots, x_n)$, is also specified. Typically, η will simply be one of the variables, for instance $\eta = x_n$.

The role of η is to indicate which state variable, or combination of state variables, will be used to communicate to other systems in an interconnection or to be fed back. (It is possible to extend the results to vector outputs as well.)

It is assumed that the state x evolves in a subset X of a Euclidean space $\mathbb{R}^n$, called the "state-space" of the system. (Technically, one requires that the subset X be contained in the closure of its interior, see refs. 1 and 2; this is a condition that is always satisfied in biochemical applications, and allows one to impose constraints such as positivity or non-negativity.) The functions f_i and h are supposed to be differentiable in all of their arguments.

The incidence graph of a system is obtained as follows. It has $n + 2$ nodes, labeled ω, η, and x_i, $i = 1, \ldots, n$. A labeled edge (an arrow with a $+$ or $-$ sign attached to it) is drawn whenever a variable x_i (or input ω) affects directly the rate of change of a variable x_j, $j \neq i$ (or the value of the output η), and a sign is attached to each label: a $+$ sign whenever the effect is positive and $-$ if the effect is negative. (By definition, we do not draw edges from any x_i to itself.) That is to say, if $f_i(x, \omega)$ is strictly increasing with respect to x_j for all (x, ω), then we draw a positive edge directed from vertex x_j to x_i; if instead $f_i(x, \omega)$ is strictly decreasing as a function of x_j for all (x, ω), then we draw a negative edge directed from vertex x_j to x_i; and if f_i is independent of x_j, no edge from x_j to x_i is drawn. Similarly for edges from the vertex ω to any vertex x_j, and from any x_j to η. [If an effect is ambiguous, because it depends on the actual values of the input or state variables, such as in the example $\dot{x}_1 = (1 - x_1)x_2 + \omega$, where $f_1(x_1, x_2, \omega) = (1 - x_1)x_2 + \omega$ is an increasing function of x_2 if $x_1 < 1$, but is a decreasing function of x_2 if $x_1 > 1$, then a graph cannot be drawn and our method as described here does not apply.] We define the sign of a path (the individual edges transversed in any direction, forward or backwards) as the product of the signs along it, and say simply that the corresponding path is positive or negative.

For example, the following system:

$$\dot{x}_1 = -x_1 + \frac{1}{1+\omega}$$
$$\dot{x}_2 = -x_1 - x_2 + x_3 - \omega$$
$$\dot{x}_3 = -x_1 + x_2 - x_3$$

with output $\eta = x_3 - x_1$ has the incidence graph shown in Fig. 6a (ignore, for now, the
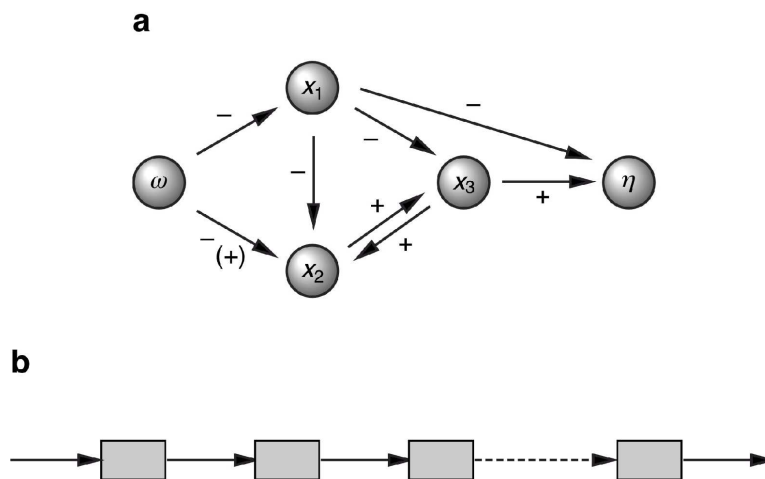
a

b

Fig. 6. (a) Example of an incidence graph. (b) A cascade of subsystems.

positive sign in parenthesis). Note, for instance, that the sign of the path x_1, x_3, x_2 is negative (one negative and one positive edge), and the sign of the path (a loop, since the beginning and endpoint coincide) ω, x_1, x_2, ω is also negative (product of three negative signs).

We define a system to be "strongly I/O monotone" provided that conditions i-iv, as described earlier, hold for the incidence graph of the system. (It is not necessary for the strict decrease or increase conditions to hold at boundary points, where some concentrations may be zero, as long as every solution of the closed loop system is guaranteed to enter the interior. Also, a far weaker condition, expressed mathematically in terms of convex cones, is sufficient, see ref. 1.) For example, a system whose graph is as shown in Fig. 6a is not monotone, because the the loop ω, x_1, x_2, ω is negative (or because there is a path from ω to η, namely ω, x_2, x_3, η, that is negative). On the other hand, if the second equation had been $\dot{x}_2 = -x_1 - x_2 + x_3 + \omega$ instead of $\dot{x}_2 = -x_1 - x_2 + x_3 - \omega$, then the graph would have a positive sign on the ω to x_2 edge (+ in parentheses), and the system would have been monotone.

Finally, we say that a system has a monostable steady-state response to constant inputs, or that it has a well-defined steady-state I/O characteristic, provided that, for each possible constant input ω, there exists a (unique) globally asymptotically stable equilibrium, denoted $k_x(\omega)$, and the nondegeneracy condition $\det Df(k_x(\omega), \omega)) \neq 0$ [Df indicates the Jacobian with respect to x] holds at the corresponding equilibrium. The

I/O characteristic is, by definition, the output corresponding to this steady state, that is $k_\eta(\omega) = h(k_x(\omega))$. The main theorem in ref. 1 is as follows. (The theorem in that reference is more general, but this special case is sufficient for our purposes.) Suppose that the system:

$$\dot{x} = f(x, \omega), \ \eta = h(x)$$

has a well-defined I/O characteristic and is strongly I/O monotone. Consider the unitary positive-feedback interconnection $\omega = \eta$:

$$\dot{x} = f(x, h(x)).$$

Then, the steady states of this closed loop system are in a 1-1 correspondence with the fixed points of the I/O characteristic. Moreover, if the derivative $k'(\omega) \neq 1$ at any fixed point ω, and if all trajectories of the sytem are bounded, then for all initial conditions, except at most those belonging to a set of measure zero, solutions converge to the set of equilibria of 5 corresponding to inputs for which $k'(\omega) < 1$. (Boundedness of trajectories is often automatic in biochemical models, because of conservation of mass and other constraints.)

A very useful fact that helps in verifying our conditions A and B is that monotonicity and existence of characteristics are always true for cascades of systems (under some mild technical mathematical conditions, see ref. 2, provided only that every individual subsystems in the cascade satisfies the requirements. Cascades are systems composed of subsystems, the output of each of which is an input to the next subsystem (Fig. 6b).

Monotonicity in the MAPK Cascade Model. We can generalize the results shown in Fig. 5b to any system with the generic form:

$$\left.\begin{array}{rcl} \dot{x}_1 &=& -\omega\theta_1(x_1) + \theta_2(M - x_1 - x_2) \\ \dot{x}_2 &=& \omega\theta_3(M - x_1 - x_2) - \theta_4(x_2) \end{array}\right\} := f(x_1, x_2, \omega),$$

where the θs denote arbitrary differentiable functions satisfying $\theta'(r) > 0$ and $\theta_i(0) = 0$ [which is true for our example where $\theta_i(r) = \frac{V_i r}{K_i + r}$, and where we take "$x_1$" to be y_1 or z_1, and "x_2" to be y_3 or z_3] and evolving on a state space given by the following triangle:

$$X = \Delta := \{[x_1, x_2] : x_1 \geq 0, \ x_2 \geq 0, \ x_1 + x_2 \leq M\}.$$

The graph associated with the system is given by that shown in Fig. 5b. Inspection of this graph proves monotonicity. See ref. 1 for generalizations to an even wider class of systems.

Parameterizing the MAPK Cascade Model. Here, we present the experimental rationale for the MAPK cascade model shown in Fig. 5, and for the particular parameters we have chosen for the model.

The basic premise of the model is that all of the enzymatic reactions reach a kinetic steady state rapidly, and therefore can be approximated by Michaelis-Menten expressions for reaction rate as a function of protein substrate concentration. A similar model (except with negative feedback rather than positive feedback) has been presented by Kholodenko (3).

The activation of p42 MAPK by MEK is assumed to occur via a nonprocessive, dual phosphorylation mechanism, based on *in vitro* studies (4-5). There is not an obligatory order for the phosphorylations, but *in vitro* the tyrosine phosphorylation generally precedes the threonine phosphorylation (4), so we suppose there are three main MAPK species—unphosphorylated MAPK (z_1), MAPK-YP (z_2), and MAPK-YP/TP (z_3), with the fourth potential species (MAPK-TP) ignored. The activities of monophosphorylated and unphosphorylated MAPK [$\sim$2% and $\sim$0.002% that of the z_3 form, respectively (6)] are ignored as well. The dephosphorylations are assumed to occur in separate steps, as indicated from experiments in *Xenopus* oocytes and extracts (7).

The mechanism of MEK activation is somewhat less well understood. The phosphorylation of MEK by Mos appears to be nonprocessive *in vitro* (8), and mutational studies suggest that MEK must be dual-phosphorylated to become fully active. However, other studies indicate that monophosphorylated MEK may possess substantial activity (9). Here we have assumed that only MEK-PP (y_3) is active.

The activation of Mos is poorly understood. It is likely to involve changes in mRNA translation (10-11), in protein stability (12), and possibly other types of regulation as well. In the absence of more detailed information on the mechanism of Mos activation, we have assumed a simplified mechanism, where Mos synthesis is directly stimulated by active MAPK (z_3).

This results in the following equations:

$$
\begin{aligned}
\dot{x} &= -\frac{V_2\,x}{K_2 + x} + vV_0 z_3 x + V_1 \\[2mm]
\dot{y}_1 &= \frac{V_6\,y_2}{K_6 + y_2} - \frac{V_3\,x\,y_1}{K_3 + y_1} \\[2mm]
\dot{y}_2 &= \frac{V_3\,x\,y_1}{K_3 + y_1} + \frac{V_5\,y_3}{K_5 + y_3} - \frac{V_4\,x\,y_2}{K_4 + y_2} - \frac{V_6\,y_2}{K_6 + y_2} \\[2mm]
\dot{y}_3 &= \frac{V_4\,x\,y_2}{K_4 + y_2} - \frac{V_5\,y_3}{K_5 + y_3} \\[2mm]
\dot{z}_1 &= \frac{V_{10}\,z_2}{K_{10} + z_2} - \frac{V_7\,y_3\,z_1}{K_7 + z_1} \\[2mm]
\dot{z}_2 &= \frac{V_7\,y_3\,z_1}{K_7 + z_1} + \frac{V_9\,z_3}{K_9 + z_3} - \frac{V_8\,y_3\,z_2}{K_8 + z_2} - \frac{V_{10}\,z_2}{K_{10} + z_2} \\[2mm]
\dot{z}_3 &= \frac{V_8\,y_3\,z_2}{K_8 + z_2} - \frac{V_9\,z_3}{K_9 + z_3}.
\end{aligned}
$$

The assumed values for the protein concentrations, rate constants, and Michaelis constants are shown in Table 1. These parameters were chosen to be consistent with experimentally determined abundance and kinetic data, where such data are available (13); to reproduce the activation and inactivation kinetics seen in *Xenopus* oocyte extracts treated with recombinant myelin basic protein-Mos (MBP-Mos) (to turn the cascade kinases on) or EDTA (to turn the cascade kinases off) (unpublished data); and, most importantly, to reproduce the experimentally determined data on the steady-state activity of p42 MAPK (z_3) as a function of the concentration of MBP-Mos in extracts (14). The

importance of this last criterion comes from the fact that our theorem shows that the shape of the characteristic for the open-loop system (Fig. 5c), which is similar to that of the measured p42 MAPK stimulus/response curve (Fig. 5d), determines the stability behavior of the closed loop system. Indeed, the model reproduces the experimental data well (Fig. 5d).

It is important to note that if nonphosphorylated MAPK (z_1) can act as a competitive inhibitor of the phosphorylation of monophosphorylated MAPK (z_2) by active MEK (y_3), and MEK is operating close to saturation, then the system will not necessarily be monotone. The same is true if bisphosphorylated MAPK (z_3) can act as a competitive inhibitor of monophosphorylated MAPK (z_2) for access to the relevant MAPK phosphatase, assuming the phosphatase is operating close to saturation.

Other Feedback Loops and Relation to Phase-Plane Analysis. For simplicity of exposition, we have described our results for feedback systems in which the output is fed back, with no further modifications, as an input (except perhaps for a multiplicative factor v). More complicated feedback loops may be studied with the same techniques, however, by a reduction to unity feedback.

Suppose that we are given a feedback loop as shown in Fig. 7a, Left, composed of two systems whose I/O characteristics are denoted f and g. System g responds to input ω, producing output z, which is fed into the system f, which in turn produces an output η, and this is used as an input $\omega = \eta$ to the first system. We may alternatively view this system as the system obtained by closing the loop ($\omega = \eta$) on the composite open-loop system formed by the cascade of the two original subsystems, see Fig. 7a, Right. Observe that the I/O characteristic $k(\omega)$ of the cascade is the composition $k = f \circ g$ of the two individual characteristics, that is, $k(\omega) = f(g(\omega))$. Steady states of the closed loop correspond to pairs ω, z such that $f(z) = \omega$ and $g(\omega) = z$, or equivalently to values ω of the input such that $f^{-1}(\omega) = g(\omega)$. We may find these steady states, therefore, by intersecting the graphs of f^{-1} and g (Fig. 7b). Stable points of the closed loop system correspond to points where the slope of g is less than the slope of f^{-1}, because the condition $k'(\omega) < 1$ when k is the composition $k(\omega) = f(g(\omega))$, is equivalent to $f'(g(\omega))g'(\omega) < 1$, which is, in turn, equivalent to $g'(\omega) < (f^{-1})'(\omega)$. [Observe that this rule is consistent with the special case when f is the identity mapping, in which case $f^{-1}(\omega) \equiv 1$ and we recover our previous condition $g'(\omega) < 1$.]

It is instructive to compare our conclusions with a routine phase plane analysis of the (very special, and only 2D) system:

$$
\begin{aligned}
\dot{z} &= -z + g(\eta) \\
\dot{\eta} &= -\eta + f(z) \,,
\end{aligned}
$$

which can be seen as the feedback interconnection of a monotone system with I/O characteristic g and a monotone system with I/O characteristic f. At any steady state (z_0, η_0) we have that $f(z_0) = \eta_0$ and $g(\eta_0) = z_0$. The Jacobian at such a point is:

$$
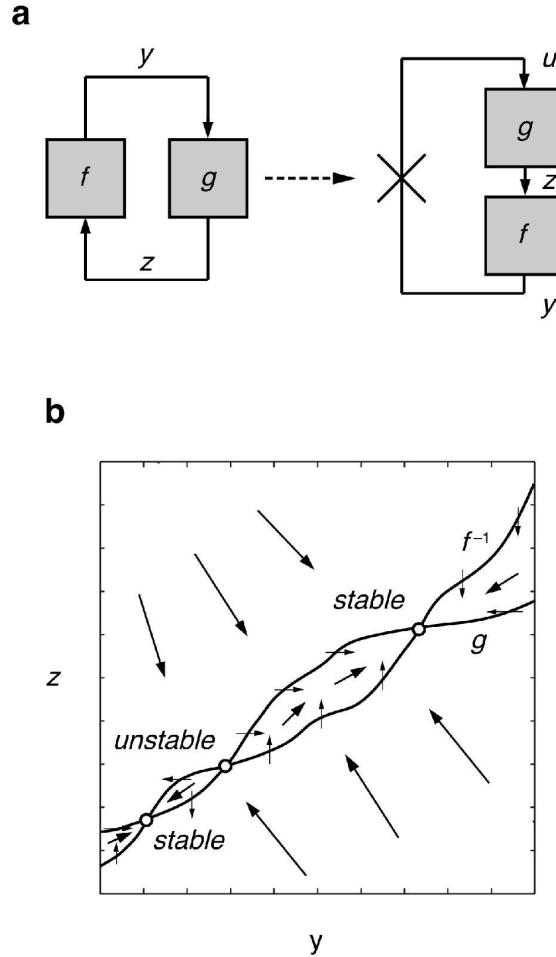\begin{pmatrix} -1 & g'(\eta_0) \\ f'(z_0) & -1 \end{pmatrix}
$$

Fig. 7. (*a*) Feedback interconnection as unity feedback. (*b*) Characteristics of g and f^{-1} are nullclines for a 2D system

which has negative trace and determinant $1 - g'(\eta_0)f'(z_0) = 1 - g'(\eta_0)f'(g(\eta_0))$. This determinant is positive, insuring (local) stability, if and only if $g'(\eta_0)f'(g(\eta_0)) < 1$, which amounts to our condition $g'(\omega) < (f^{-1})'(\omega)$ at $\omega = \eta_0$.

In fact, global stability can be analyzed in this case as well. We may draw nullclines and sketch vector field directions very easily (Fig. 7*b*). It is then clear from this sketch that there is global stability to the states at which the condition $g'(\omega) < (f^{-1})'(\omega)$. Our results hold for systems in arbitary dimensions, and not just in this special form, provided that monotonicity and existence of I/O characteristics have been verified.

Further Remarks: Robustness and Other Feedback Structures. Our method is fairly robust to biochemically plausible variations in the models being considered. It can be mathematically shown that the form of the characteristic is preserved under small perturbations in the parameters of a model. Moreover, in the MAPK example, we used a standard model based on quasi-steady state assumptions; if these fast intermediate reactions are kept in the model, one may still apply our methodology.

Complex signaling and regulatory networks involve multiple and interlocked positive and feedback loops. Much further research will be needed to obtain a complete set of tools to analyze such complex systems in their full generality. Our approach is based on the idea of breaking up loops and reconstituting the system by analyzing the various interconnections. In particular, negative feedback interconnections, which may give rise to oscillations, are studied in detail in ref. 2.

Table 1. Kinetic parameters used in the MAPK cascade model

	Parameter	Value	Source
y_{tot}	total MEK concentration	1,200 nM	Experimentally determined (13)
z_{tot}	total p42 MAPK concentration	300 nM	Experimentally determined (13)
V_0	... $\xrightarrow{\text{MAPK-PP}}$ Mos	0.0015 sec$^{-1}\cdot$nM^{-1}	Arbitrary
V_1	... $\rightarrow$ Mos	0.000002 sec^{-1}	Arbitrary
V_2	Mos $\rightarrow$ ...	1.2 nm$\cdot$sec^{-1}	Arbitrary
K_2	Mos $\rightarrow$ ...	200 nM	Arbitrary
V_3	MEK $\xrightarrow{\text{Mos-P}}$ MEK-P	0.064 sec^{-1}	Consistent with kinetics of MEK activation in Mos-treated extracts (unpublished data)
K_3	MEK $\xrightarrow{\text{Mos-P}}$ MEK-P	1,200 nM	Arbitrary; equal to the measured total abundance of MEK (13)
V_4	MEK-P $\xrightarrow{\text{Mos-P}}$ MEK-PP	0.064 sec^{-1}	Consistent with kinetics of MEK activation in Mos-treated extracts (unpublished data)
K_4	MEK-P $\xrightarrow{\text{Mos-P}}$ MEK-PP	1,200 nM	As for K_3.
V_5	MEK-PP $\rightarrow$ MEK-P	5 nm$\cdot$sec^{-1}	Consistent with kinetics of MEK inactivation in EDTA-treated extracts (unpublished data)
K_5	MEK-PP $\rightarrow$ MEK-P	1,200 nM	As for K_3.
V_6	MEK-P $\rightarrow$ MEK	5 nm$\cdot$sec^{-1}	As for V_5.
K_6	MEK-P $\rightarrow$ MEK	1,200 nM	As for K_3.
V_7	MAPK $\xrightarrow{\text{MEK-PP}}$ MAPK-P	0.06 sec^{-1}	Experimental estimates with activated recombinant MEK are $\sim$0.024 sec^{-1} (ref. 15)
K_7	MAPK $\xrightarrow{\text{MEK-PP}}$ MAPK-P	300 nM	Experimental estimates with activated recombinant MEK are $\sim$330 nM (15)
V_8	MAPK-P $\xrightarrow{\text{MEK-PP}}$ MAPK-PP	0.06 sec^{-1}	As for V_7.
K_8	MAPK-P $\xrightarrow{\text{MEK-PP}}$ MAPK-PP	300 nM	Experimental estimates with activated recombinant MEK are $\sim$330 nM (15)
V_9	MAPK-PP $\rightarrow$ MAPK-P	5 nm$\cdot$sec^{-1}	Together with the assumed value of K_9 (300 nM), this implies a half-time of $\sim$50 sec for this dephosphorylation reaction. Experiments indicate an apparent half-time on the order of 5 min (7).
K_9	MAPK-PP $\rightarrow$ MAPK-P	300 nM	Based on unpublished evidence.
V_{10}	MAPK-P $\rightarrow$ MAPK	5 nm$\cdot$sec^{-1}	As for V_9.
K_{10}	MAPK-P $\rightarrow$ MAPK	300 nM	As for K_9.

1. Angeli, D. & Sontag, E.D. (2003) *Syst. and Control Lett.*, in press.

2. Angeli, D. & Sontag, E.D. (2003) *IEEE Trans. Autom. Control* **48**, 1684–1698.

3. Kholodenko, B.N. (2000) *Eur. J. Biochem.* **267**, 1583-1588.

4. (1997) Ferrell, J.E., Jr. & Bhatt, R.R. *J. Biol. Chem.* **272**, 19008-19016.

5. Burack, W.R. & Sturgill, T.W. (1997) *Biochemistry* **36**, 5929-5933.

6. Lew, J. (2003) *Biochemistry* **42**, 849-856.

7. Sohaskey, M.L. & Ferrell, J.E., Jr. (1999) *Mol. Biol. Cell* **10**, 3729-3743.

8. Resing, K.A., Mansour, S.J., Hermann, A.S., Johnson, R.S., Candia, J.M., Fukasawa, K., Vande Woude, G.F. & Ahn, N.G. (1995) *Biochemistry* **34**, 2610-2620.

9. Alessi, D.R., Saito, Y., Campbell, D.G., Cohen, P., Sithanandam, G., Rapp, U., Ashworth, A., Marshall, C.J. & Cowley, S. (1994) *EMBO J.* **13**, 1610-1619.

10. Barkoff, A., Ballantyne, S. & Wickens, M. (1998) *EMBO J.* **17**, 3168-3175.

11. Howard, E.L., Charlesworth, A., Welk, J. & MacNicol, A.M. (1999) *Mol. Cell. Biol.* **19**, 1990-1999.

12. Castro, A., Peter, M., Magnaghi-Jaulin, L., Vigneron, S., Galas, S., Lorca, T. & Labbe, J.C. (2001) *Mol. Biol. Cell* **12**, 2660-2671.

13. Ferrell, J.E., Jr. (1996) *Trends Biochem. Sci.* **21**, 460-466.

14. Huang, C.-Y.F. & Ferrell, J.E., Jr. (1996) *Proc. Natl. Acad. Sci. USA* **93**, 10078-10083.

15. Mansour, S.J., Candia, J.M., Matsuura, J.E., Manning, M.C. & Ahn, N.G. (1996) *Biochemistry* **35**, 15529-15536.